Supporting Information

Highly Efficient Perovskite Solar Cells with Gradient Bilayer Electron Transport Materials

Xiu Gong[a], *Qiang Sun*[a], *Shuangshuang Liu*[a], *Peizhe Liao*[a], *Yan Shen*[a], *Carole Grätzel*[b], *Shaik M. Zakeeruddin*[b], *Michael Grätzel*[b] *and Mingkui Wang**[,a]

[a] Wuhan National Laboratory for Optoelectronics, School of Optical and Electronic Information, Huazhong University of Science and Technology, Wuhan 430074, Hubei, P. R. China

[b] Laboratoire de Photonique et interfaces (LPI), Ecole Polytechnique Federale de Lausanne CH-1015 Lausanne, Switzerland

* Corresponding author E-mail: mingkui.wang@mail.hust.edu.cn (M.W.)

Device Fabrication

The etched fluorine-doped tin oxide (FTO) glass was cleaned using detergent water, acetone, ethanol and deionized water, separately in ultrasonic bath for 15 min each, then dried by nitrogen. The FTO substrates underwent an UV-O_3 treatment for 20 min before they were used for spin-coating F:SnO_2 ethanol solution. A F:SnO_2 ETL with 50nm thickness was prepared by spin coating F：SnO_2 solution with different F doping ratios and annealing temperature at 4000 rpm for 30s in ambient condition, and achieving $(F:Sn_2O)_{180}$, $(F:Sn_2O)_{380}$ and $(F:Sn_2O)_{500}$ film with different F doping ratios, and the bi-layer composition of 20nm $(F:Sn_2O)_{380}$ with 0.2 F doping and 40nm $(F:Sn_2O)_{180}$ with 0.2 F doping. After cooling to room

temperature, the samples were treated again with UV-O_3 for 30 min and transferring into a glovebox for perovskite deposition. FAI (1 M), PbI_2 (1.1 M), MABr (0.2 M), and $PbBr_2$ (0.2 M) were dissolved in a 4:1 (v:v) mixture of anhydrous DMF : DMSO (Acros) to prepare the $(FAPbI_3)_{0.85}(MAPbBr_3)_{0.15}$ perovskite precursor solution. The mixture solution was deposited through a one-step spin coating process (30 s at 6000 rpm) with dripping of chlorobenzene as anti-solvent, 15-17 s before the end. All the perovskite layers annealed at 120 ℃ for 45 min. 72.3 mg/mL spiro-OMeTAD of chlorobenzene with 28.8 μL TBP and17.5 μL Li-TFSI/acetonitrile (520 mg mL-1) was spin-coated on the perovskite films at 4000 rpm for 40 s. Finally, a 100 nm gold counter electrode was deposited by thermal evaporation. The thickness of each layer was about 50 nm for F:SnO_2 ETL, 500 nm for perovskite layer, 200 nm for spiro-OMeTAD HTL, and 100 nm for gold electrode.

Device Characterization

UPS measurements were performed to define the change of energy levels by a Kratos AXIS Ultra-DLD ultra-high-vacuum photoemission spectroscopy system with an Al Kα radiation source. The surface morphology for ETLs and perovskite films were characterized with a field-emission scanning elect (FE-SEM). Energy dispersive spectrometer (EDS) images were obtained using FEI Nova Nano SEM 450. TEM and HRTEM analysis were carried out on a FEI OSIRIS microscope. The X-ray diffraction spectrometry pattern was measured using Shimadzu XRD-6100 diffractometer (Cu K a radiation). Films surface roughness was performed using tapping mode atomic force microscopy (Veeco multimode instrument). Hall measurements were conducted by a Lake Shore 7704 Hall Measurement System. Steady-state photoluminescence (PL) and time-resolved PL decay were conducted by time-resolved luminescence decays with time-correlated single photo counting system (PicoHarp 300, PicoQuant GmbH). A laser beam with an excitation wavelength of 532 nm was used to excite the perovskite layer from the air side. The excitation light source was Ti: Sapphire laser (Mira

900, Coherent; 76 MHz, 130 fs). The nanosecond transient absorption spectroscopy was obtained by were obtained by focusing the fundamental beams onto a sapphire plate (contained in LP920, Edinburgh Instruments). The transmitted probe light from the samples was collected and focused on the broadband VIS-NIR detector for recording the time-resolved excitation induced difference spectrum (ΔOD). For details principle, please refer to previous literatures.[1] The photocurrent density-voltage (J-V) characteristics of PSCs were measured under 1 sun illumination using a programmable Keithley 2400 digital source meter with AM 1.5 G simulated solar light. The incident photon conversion efficiency (IPCE) measurement was obtained under alternating current (AC) model (130 Hz). The electronic impedance spectra (EIS) characteristics were recorded the Autolab PGSTAT 30 (Eco Chemie B.V., Utrecht, The Netherlands) and the frequency range from 0.01 Hz to 1 MHz with oscillating amplitude of 10 mV. The Z-view software (v2.8 b, Scribner Associates Inc.) was used to analyze the impedance spectra.

Table of Contents

Table S1. A brief summary of the morphology and the energy band controls of the electron transporting layer by different element doping based planar perovskite solar cell.

ETLs	Cell Configuration	V_{oc} (V)	J_{sc} (mA/cm^2)	FF	PCE (%)	Reference
Y-doped TiO_2	FTO/Y: TiO_2/$MAPbI_3$/Spiro	1.13	22.75	75.01	19.3	Science 2014, 345, 542-546
Zr-doped TiO_2	ITO/Zr: TiO_2/$MAPbI_3$/Spiro	1.021	20.3	76	15.7	J. Mater. Chem. A 2015, 3, 9108
Mg-doped TiO_2	FTO/Mg:TiO_2compact/TiO_2 $MAPbI_3$ /Spiro	1.08	18.34	62	12.28	Appl. Phys. Lett. 2015, 106, 121104.
CQD-doped TiO_2	ITO/TiO_2(CQD)/$MAPbI_3Cl_{3-x}$ /spiro	1.139	21.36	78	18.89	Nano Lett. 2017, 7, 2328
N-doped ZnO	ITO/ZnO/N:ZnO/$MAPbI_3$/Spiro	0.995	22.1	74	16.27	Adv. Energy Mater. 2015, 5, 1500568.
Mg-doped ZnO	ITO/Mg:ZnO/$MAPbI_3$/Spiro	0.99	22.7	68	15.3	Appl. Phys. Lett. 2015, 107, 073507
Al-doped ZnO	ITO/Al:ZnO/$MAPbI_3$/Spiro	1.045	15.1	76	12	Nanoscale 2014, 6, 9127
$TiCl_4$-SnO_2	FTO/SnO_2-$TiCl_4$/$MAPbI_3Cl_{3-x}$/Spiro	0.997	20.0	67.0	14.69	Adv. Funct. Mater. 2015, 25, 7200
Surface modified ETL	FTO/NiO/$MAPbI_3$/C60/SnO_2/Ag .	1.12	21.8	77	18.8	Adv. Mater. 2016, 28, 6478
	FTO/ MgO /SnO_2/$MAPbI_3$/Spiro	1.10	22.7	73	18.23	Adv. Sci. 2017, 1700031
	FTO/SnO_2/SAM/$MAPbI_3$/Spiro	1.16	21.93	72	18.32	J. Mater. Chem. A 2017, 5, 1658
	FTO/SnO_2/PCBM/$MAPbI_3$/ Spiro	1.11	21.41	76.20	18.17	J. Mater. Chem. A, 2016, 4, 14276
Li-doped SnO_2	FTO/Li:SnO_2/$MAPbI_3$/Spiro	1.106	23.27	70.71	18.20	Nano Energy 2016, 26, 208
Sb-doped SnO_2	ITO/Sb: SnO_2/$MAPbI_3$ /Spiro	1.06	22.6	72	17.2	ChemSusChem 2016, 9, 2689
Nb-doped SnO_2	FTO/Nb:SnO_2/$(FAPbI_3)_{0.85}$($MAPbBr_3$)$_{0.15}$ /Spiro	1.08	22.36	72.7	17.57	ACS Appl. Mater. Interfaces 2017, 9, 2421
Y-doped SnO_2	FTO/Y: SnO_2/$MAPbI_3$/Spiro	1.08	22.55	71	17.29	Small 2017, 13, 1601769
Mg-doped SnO_2	FTO/Mg: SnO_2/$MAPbI_3$/Spiro	0.991	20.92	66.8	13.56	J. Mater. Chem. A 2016, 4, 8374
F-doped SnO_2 bilayer ETL	FTO/$(F:SnO_2)_{380}$-0.2/$(F:SnO_2)_{180}$-0.2/ Perovskite /Spiro	1.13	22.92	78.05	20.20	This work

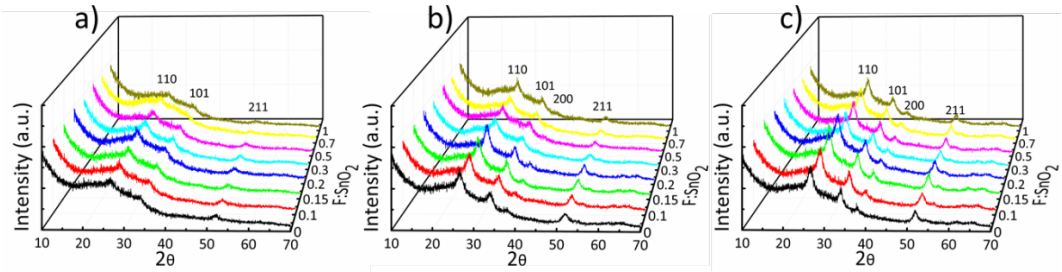

Figure S1. XRD patterns of F:SnO_2 thin films deposited on quartz glass substrate: a) $(F:SnO_2)_{180}$, b) $(F:SnO_2)_{380}$ and c) $(F:SnO_2)_{500}$.

From the figure S1, one can see that the annealing temperature rises up to 380 ^oC, the (200) diffraction peak at 37.95° starts to emerge, especially at 500 ^oC, becomes obvious. In addition, the intensity of (200) peak of the F-doped SnO_2 films slightly increases with fluorine content to 0.2 ratios, and then decreases gradually at high doping ratios. For instance, it has begun to vanish in the $(F:SnO_2)_{380}$ film at doping ratio from 0.5 to 1 as shown in Figure S1b, which indicates that 0.2 is the optimum doping ratio, which was used in the following in-depth study.

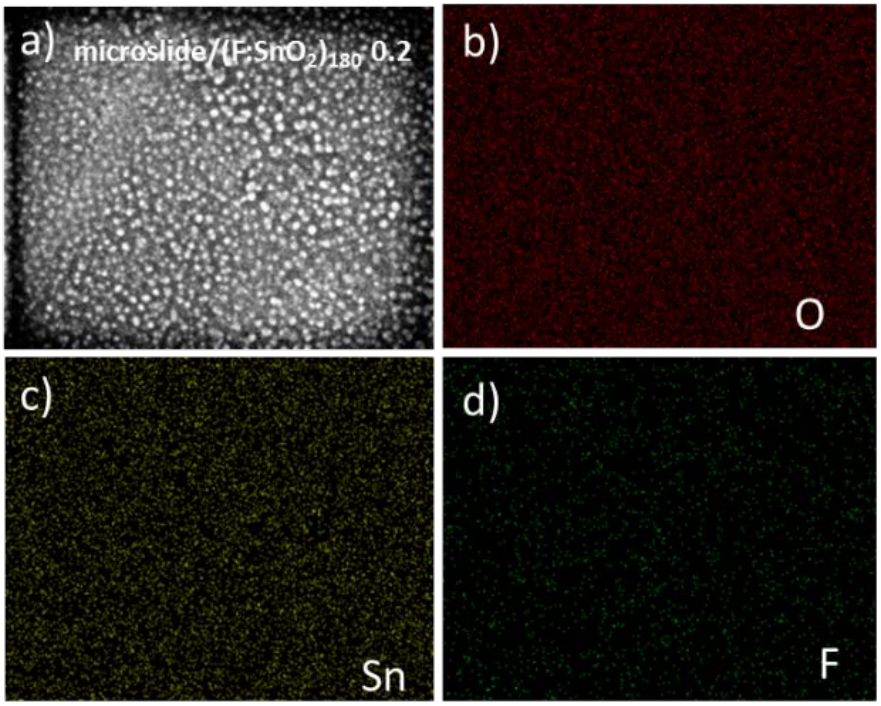

Figure S2. a) SEM morphology of $(F:SnO_2)_{180}$ film with 0.2 F doping, and EDS mapping images of $(F:SnO_2)_{180}$ film with 0.2 F doping for elements: b) O, c) Sn and d) F.

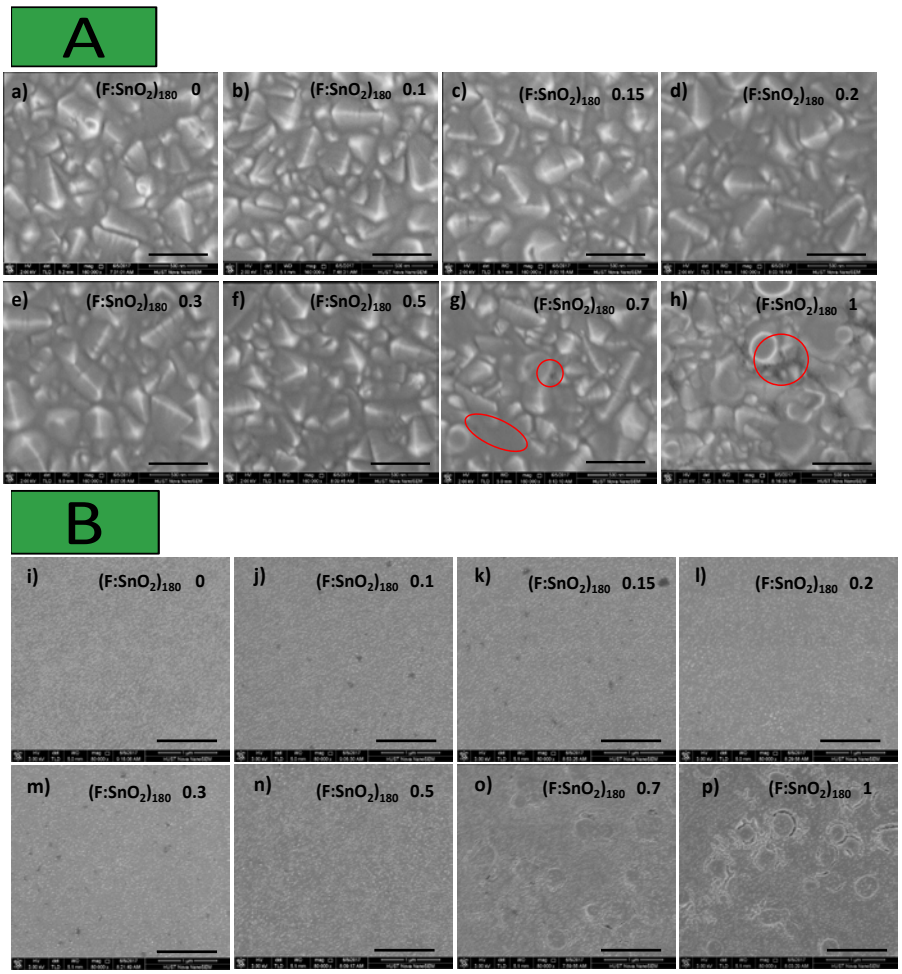

Figure S3. Top view SEM images of $(F:SnO_2)_{180}$ film with varied F doping ratio . a) 0, b) 0.1, c) 0.15, d) 0.2, e) 0.3, f) 0.5, g) 0.7 and h) 1 on FTO substrate, all scale bars are 500 nm. i) 0, j) 0.1, k) 0.15, l) 0.2, m) 0.3, n) 0.5, o) 0.7 and p) 1 on glass substrate, all scale bars are 1 um.

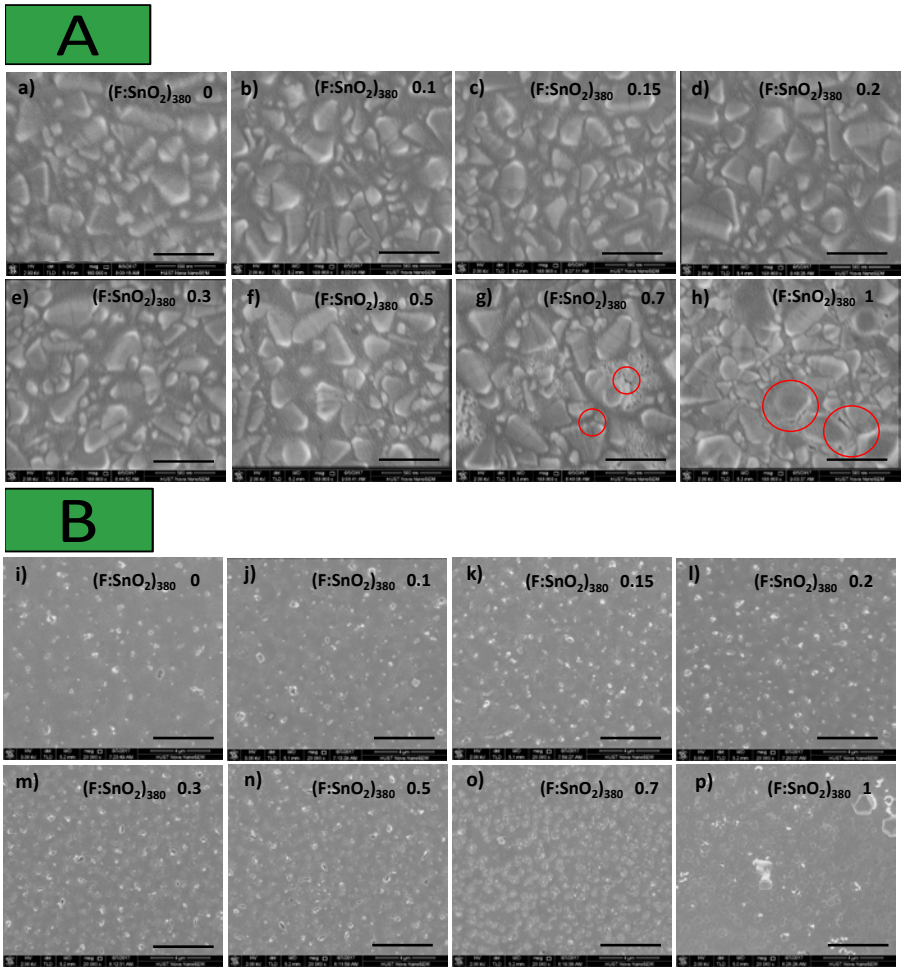

Figure S4. Top view SEM images of $(F:SnO_2)_{380}$ film with varied F doping ratio . a) 0, b) 0.1, c) 0.15, d) 0.2, e) 0.3, f) 0.5, g) 0.7 and h) 1 on FTO substrate and all scale bars are 500 nm. i) 0, j) 0.1, k) 0.15, l) 0.2, m) 0.3, n) 0.5, o) 0.7 and p) 1 on glass substrate, all scale bars are 4 um.

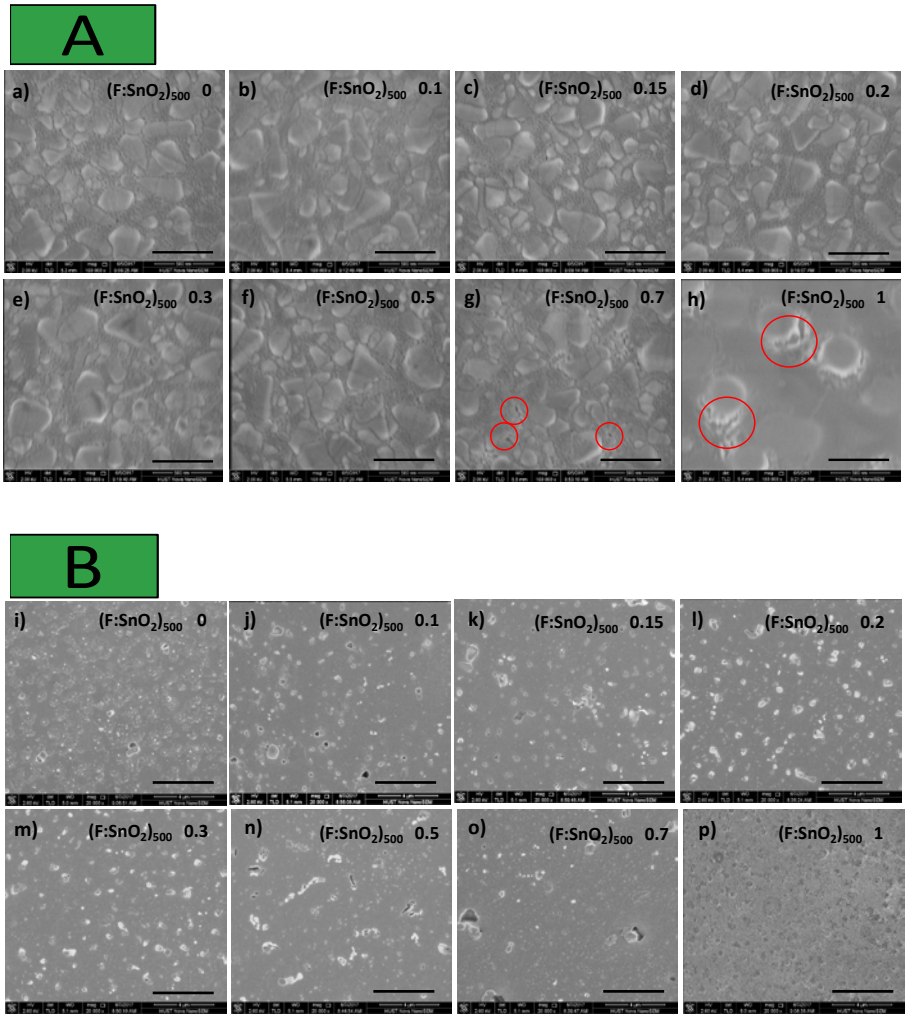

Figure S5. Top view SEM images of $(F:SnO_2)_{500}$ film with varied F doping ratio. a) 0, b) 0.1, c) 0.15, d) 0.2, e) 0.3, f) 0.5, g) 0.7 and h) 1 on FTO. All scale bars are 500 nm. i) 0, j) 0.1, k) 0.15, l) 0.2, m) 0.3, n) 0.5, o) 0.7 and p) 1 on glass substrate, all scale bars are 4 um.

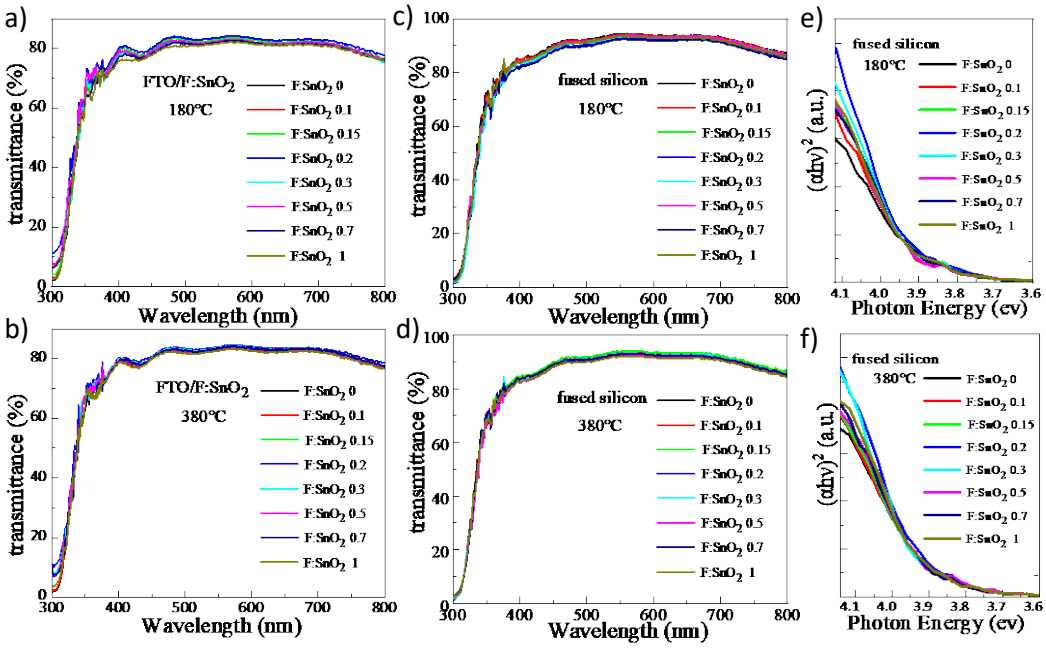

Figure S6. Transmission spectra of F:SnO_2 thin films deposited on FTO and quartz glass substrate: (a, c) $(F:SnO_2)_{180}$; (b, d) $(F:SnO_2)_{380}$. (e, f) the $(ahv)^2$ versus hv plots of F:SnO_2 thin films corresponding to (c,d).

Table S2. Bandgap of different ETL materials

E_g	0	0.1	0.15	0.2	0.3	0.5	0.7	1
$(F:SnO_2)_{180}$	3.87	3.89	3.91	3.92	3.91	3.89	3.89	3.89
$(F:SnO_2)_{380}$	3.88	3.90	3.92	3.94	3.92	3.91	3.90	3.90

Table S3 Carrier density (n, cm^{-3}), resistivity (R, Ω cm)， electrical conductivity (σ, μs cm^{-1}), mobility (μ, $cm^2\ V^{-1}\ s^{-1}$) and the change of Fermi levels ($\triangle E_f$, meV) for $(F:SnO_2)_{180}$ and $(F:SnO_2)_{380}$, respectively.

$(F:SnO_2)_{180}$	0	0.1	0.15	0.2	0.3	0.5	0.7	1
n(cm^{-3})	2.03×10^{14}	3.09×10^{14}	6.44×10^{14}	1.90×10^{15}	3.41×10^{14}	1.62×10^{14}	8.85×10^{13}	2.76×10^{13}
R (Ω cm)	2.68×10^{3}	1.87×10^{3}	7.89×10^{2}	2.69×10^{2}	1.57×10^{3}	3.78×10^{3}	8.94×10^{3}	1.36×10^{4}
σ （μs cm^{-1}）	3.73×10^{2}	5.34×10^{2}	1.27×10^{3}	3.72×10^{3}	6.37×10^{2}	2.65×10^{2}	1.12×10^{2}	7.35×10^{1}
μ ($cm^2\ V^{-1}\ s^{-1}$)	12.15	26.4	12.48	11.52	13.53	10.5	8.13	12.05
$\triangle E_f$ (meV)	---	10	30	58	35	13	-21	-51

$(F:SnO_2)_{380}$	0	0.1	0.15	0.2	0.3	0.5	0.7	1
n(cm^{-3})	3.49×10^{15}	2.43×10^{16}	5.07×10^{16}	9.07×10^{16}	4.86×10^{16}	1.35×10^{16}	1.10×10^{16}	2.38×10^{15}
R (Ω cm)	9.11×10^{1}	6.18×10^{1}	1.42×10^{1}	5.34	4.83×10^{1}	1.26×10^{2}	5.03×10^{2}	6.52×10^{2}
σ （μs cm^{-1}）	1.09×10^{4}	1.62×10^{4}	7.05×10^{4}	1.87×10^{5}	2.07×10^{4}	7.93×10^{3}	1.98×10^{3}	1.53×10^{3}
μ ($cm^2\ V^{-1}\ s^{-1}$)	17.6	4.18	7.40	11.63	2.69	3.35	1.09	3.92
$\triangle E_f$ (meV)	---	50	69	84	68	35	30	-10

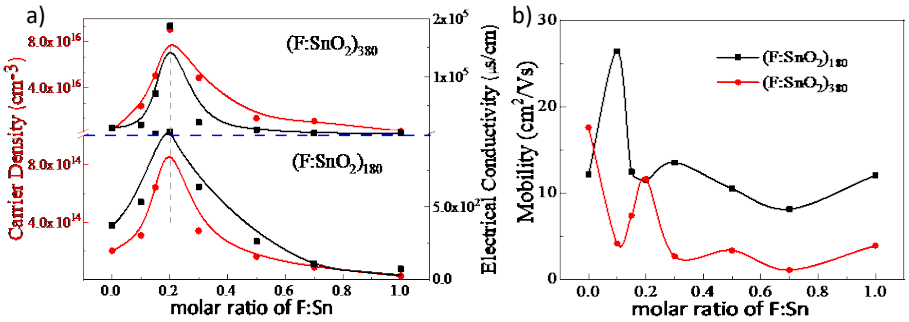

Figure S7. a) Carrier density and electrical conductivity, and b) mobility of the $(F:SnO_2)_{180}$ and $(F:SnO_2)_{380}$ thin films deposited on quartz glass substrate as a function of F content. The $(F:SnO_2)_{380}$ and $(F:SnO_2)_{180}$ thin film distribute at above and below of the blue line, and the red line and black line representing carrier density and electrical conductivity in Figure S7a.

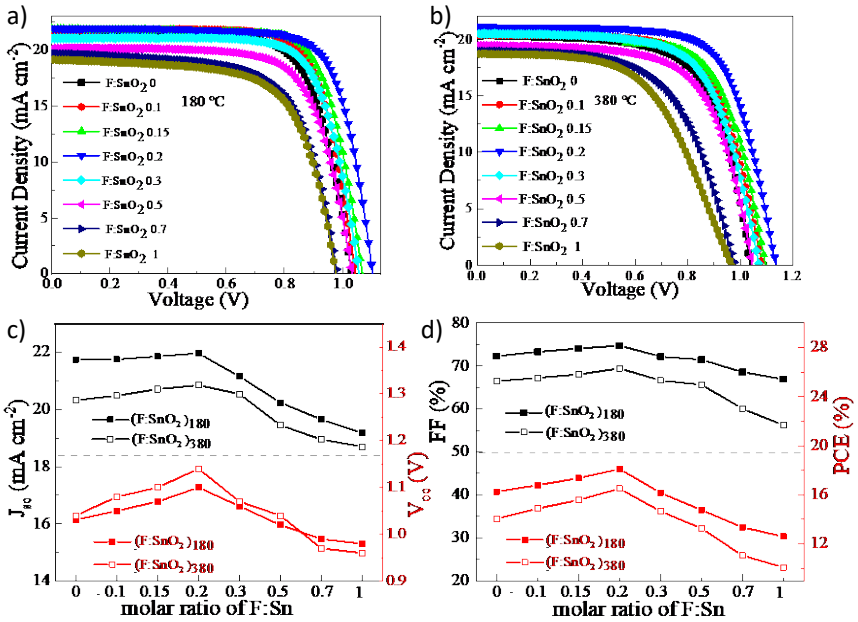

Figure S8. J-V curves of PHJ PSCs with different F:SnO_2 thin film under AM 1.5 G illumination of 100 mW cm^{-2}: a) $(F:SnO_2)_{180}$, b) $(F:SnO_2)_{380}$, c) J_{SC} and V_{OC} versus F content, black for J_{SC} and red for V_{OC}. d) FF and PCE versus F content, black for FF and red for PCE.

Table S4. Work function of different ETL materials (deposited onto FTO substrate) measured by Kelvin probe in air.

W_F	0	0.1	0.15	0.2	0.3	0.5	0.7	1
$(F:SnO_2)_{180}$	4.58	4.58	4.60	4.55	4.58	4.62	4.6	4.67
$(F:SnO_2)_{380}$	4.57	4.53	4.52	4.50	4.49	4.46	4.42	4.47

Note: Work function of FTO is 4.67

Table S5. The cell performance of perovskite solar cells based on $(F:SnO_2)_{180}$ with varied ratio of F doping.

Device $(F:SnO_2)_{180}$	J_{sc} (mA/cm^2)	V_{oc} (V)	$V_{oc\text{-}AVE}$ (V)	FF (%)	PCE (%)	PCE_{AVE} (%)
0	21.74	1.03	1.02±0.02	72.28	16.25	15.80±0.24
0.1	21.75	1.05	1.03±0.03	73.45	16.78	16.01±0.98
0.15	21.85	1.07	1.05±0.01	74.06	17.36	16.48±0.88
0.2	21.96	1.10	1.05±0.02	74.76	18.10	17.16±0.84
0.3	21.15	1.06	1.02±0.05	72.17	16.17	15.93±0.25
0.5	20.24	1.02	0.95±0.07	71.47	14.76	14.44±0.32
0.7	19.65	0.99	0.87±0.12	68.58	13.35	12.16±0.76
1	19.18	0.98	0.75±0.23	66.90	12.59	12.34±1.25

Table S6. The cell performance of perovskite solar cells based on $(F:SnO_2)_{380}$ with varied ratio of F doping.

Device $(F:SnO_2)_{380}$	J_{sc} (mA/cm^2)	V_{oc} (V)	$V_{oc\text{-}AVE}$ (V)	FF (%)	PCE (%)	PCE_{AVE} (%)
0	20.32	1.04	1.02±0.02	66.46	14.04	13.58±0.46
0.1	20.48	1.08	1.03±0.03	67.21	14.87	14.55±0.32
0.15	20.71	1.10	1.05±0.04	68.02	15.58	14.61±0.97
0.2	20.85	1.14	1.07±0.05	69.43	16.50	16.38±0.12
0.3	20.54	1.07	1.05±0.02	66.60	14.65	13.89±0.76
0.5	19.43	1.04	1.02±0.02	65.67	13.27	12.18±1.03
0.7	18.95	0.97	0.85±0.12	60.07	11.05	10.69±0.36
1	18.70	0.96	0.78±0.18	56.21	10.09	9.54±0.55

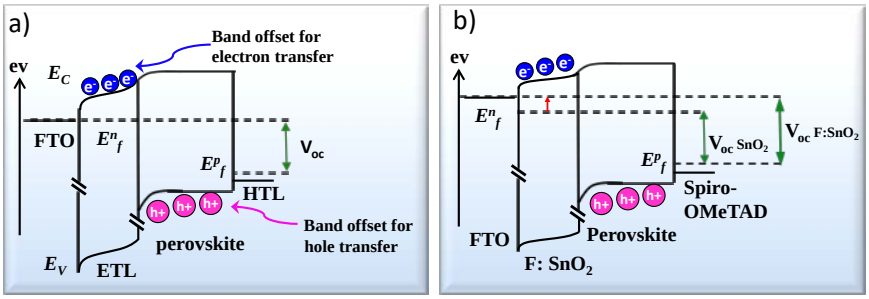

Figure S9. a) Band offset diagram of ETL–perovskite as determined by Fermi energy of ETL under illumination. b) Band diagram of the perovskite solar cells based on SnO_2 and F:SnO_2 ETLs under illumination. E^n_f: fermi energy of ETL; E^p_f: fermi energy of HTL; E_C: conduction band; E_V: valence band.

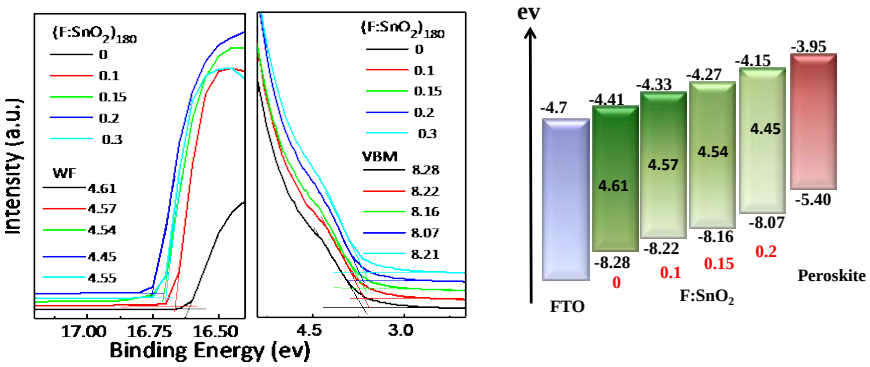

Figure S10. UPS characterization of (F: SnO_2)$_{180}$ films and corresponding schematic band energy levels diagram of (F: SnO_2)$_{180}$ with respect to the FTO and Perovskite.

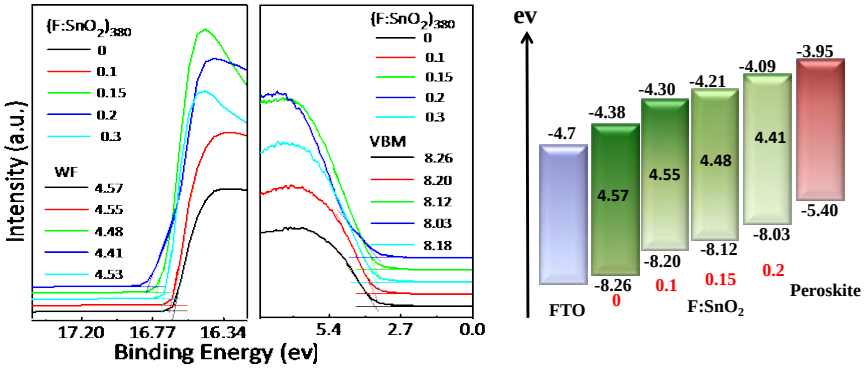

Figure S11. UPS characterization of (F: SnO_2)$_{380}$ films and corresponding schematic band energy levels diagram of (F: SnO_2)$_{380}$ with respect to the FTO and Perovskite.

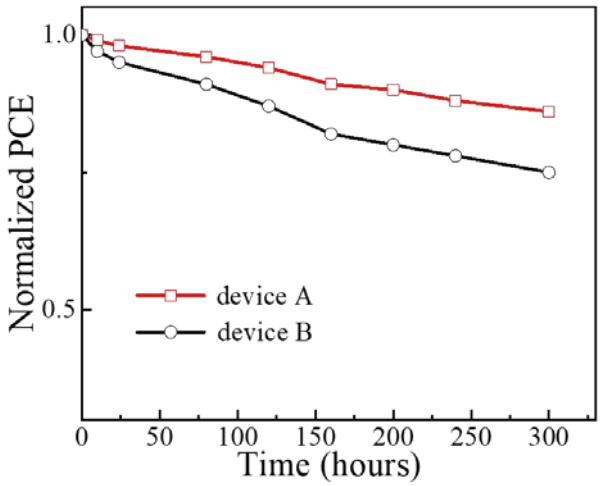

Figure S12. Stability of perovskite solar cells device A based on bi-layer ETL and device B based on undoped SnO_2 substrate measured under one sun illumination. Simple encapsulated devices are placed in the air with humidity of 40% -50%, the testing humidity of PCE greater than 60%.

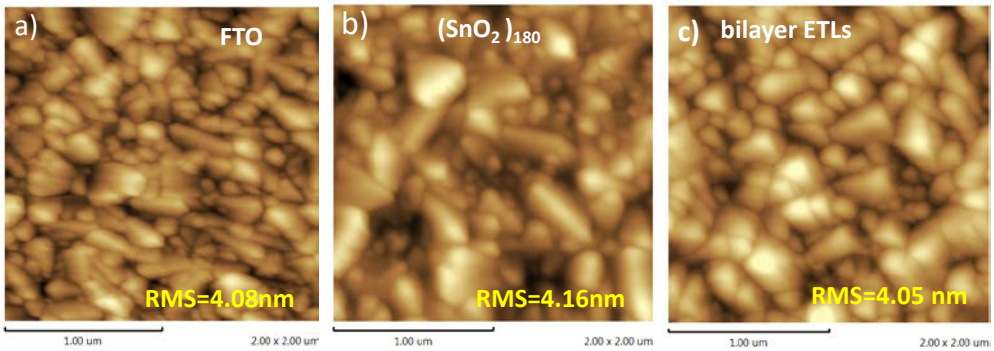

Figure S13. a) AFM images of FTO, b) undoped $(SnO_2)_{180}$ film and c) bilayer ETLs. RMS is the root-mean-square roughness values.

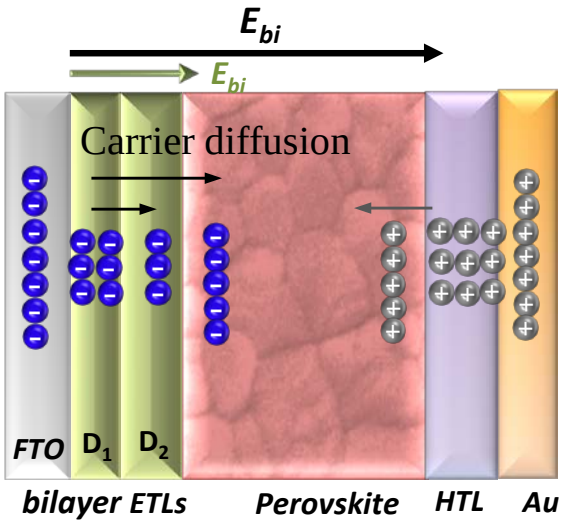

Figure S14. Schematic of the built-in field in bilayer ETLs based devices.

The carrier concentration of D_1 layers is greater than that D_2 in the bilayer ETLs. This difference could produce carrier diffusion (indicated with the red dotted lines arrows) that further contributes the built-in electric field E_{bi} (indicated with the red lines arrows) for efficient the carrier extraction. Furthermore, an increased conductivity by F doping expedites electron transfer from perovskite to bilayer ETLs and reduces interfacial charge recombination, which improves device V_{OC} as payback. Therefore, the unique bilayer ETLs concept results in enhancements of PCE performance due to the dual functions of the individual ETLs.

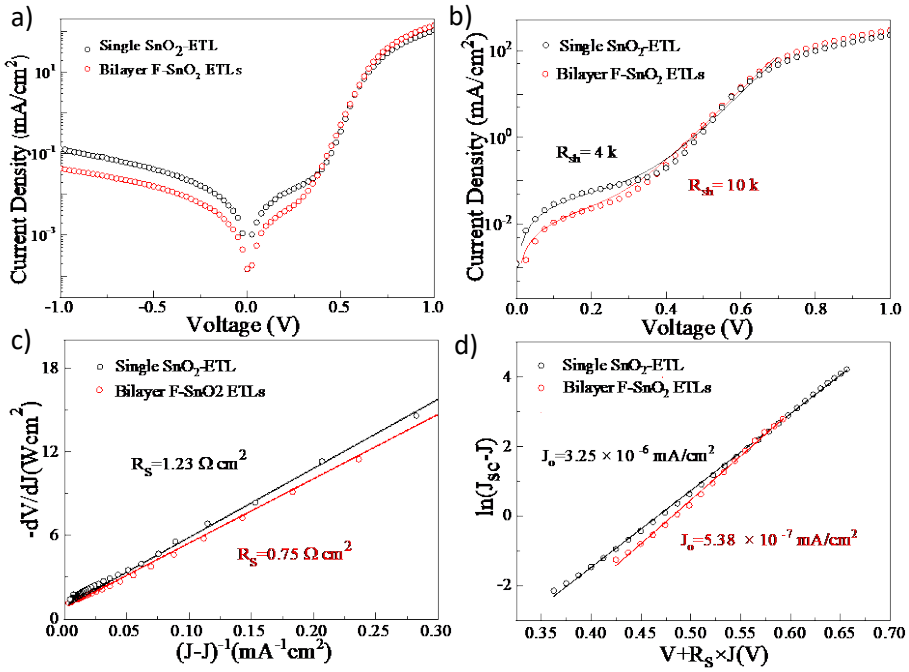

Figure S15. a) Dark J-V curves of perovskite solar cells with bi-layer ETL and undoped SnO_2, b) the corresponding fitted curves of dark J-V curves, c) plots of -dV/dJ vs $(J_{sc}-J)^{-1}$ and the linear fitting curves. d) plots of $\ln(J_{sc}-J)$ against $V+R_s J$ and the linear fitting curves[2-4]. Empty circles and solid lines represent measured data and fit result, respectively

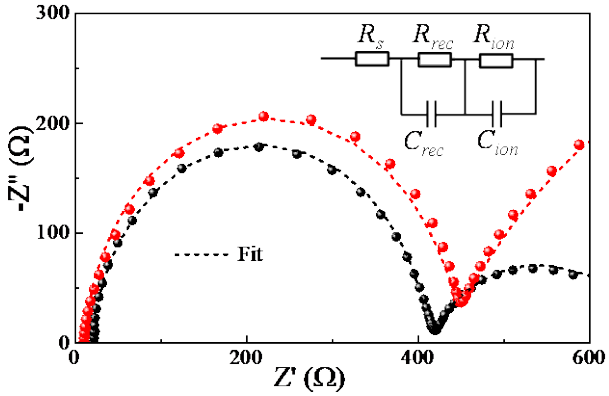

Figure S16. Nyquist plots of perovskite solar cells based on different electron transport layers under illumination.

References

(1) Li, H.; Shi, W.; Huang, W.; Yao, E.-P.; Han, J.; Chen, Z.; Liu, S.; Shen, Y.; Wang, M.; Yang, Y. *Nano Lett.* **2017,** *17*, 2328-2335.

(2) Shi, J.; Dong, J.; Lv, S.; Xu, Y.; Zhu, L.; Xiao, J.; Xu, X.; Wu, H.; Li, D.; Luo, Y. *Appl. Phys.Lett.* **2014**, *104*, 6050-19090.

(3) Lee, J. W.; Kim, D. H.; Kim, H. S.; Seo, S. W.; Cho, S. M.; Park, N. G. *Adv. Energy Mater.* **2015**, *5*,1501310.

(4) Liao P.-Z.; Zhao X.-J,; Li G.-L.; Shen, Y.; Wang, M. *Nano-Micro Lett* **2018**, *10*, 1-8.